Earth and Planetary Science Letters 506 (2019) 455–465

Contents lists available at ScienceDirect

Earth and Planetary Science Letters

www.elsevier.com/locate/epsl

Temperature signals in tree-ring oxygen isotope series from the northern slope of the Himalaya

Ru Huang [a,c], Haifeng Zhu [a,b,*], Eryuan Liang [a,b], Jussi Grießinger [d], Jakob Wernicke [d], Wusheng Yu [a,b], Philipp Hochreuther [d], Camille Risi [e], Yijian Zeng [f], Astrid Fremme [g], Harald Sodemann [g], Achim Bräuning [d]

[a] Key Laboratory of Alpine Ecology, Institute of Tibetan Plateau Research, Chinese Academy of Sciences, Beijing 100101, China
[b] CAS Center for Excellence in Tibetan Plateau Earth Sciences, Beijing 100101, China
[c] University of Chinese Academy of Sciences, Beijing 10049, China
[d] Institute of Geography, University of Erlangen-Nuremberg, Wetterkreuz 15, 91058 Erlangen, Germany
[e] Laboratoire de Météorologie Dynamique, Institut Pierre Simon LaPlace, Centre National de la Recherche Scientifique, 75252 Paris, France
[f] Department of Water Resources, ITC Faculty of Geo-Information Science and Earth Observation, University of Twente, Enschede 7514 AE, the Netherlands
[g] Geophysical Institute, University of Bergen and Bjerknes Centre for Climate Research, 5007 Bergen, Norway

ARTICLE INFO

Article history:
Received 17 February 2018
Received in revised form 30 October 2018
Accepted 2 November 2018
Available online 23 November 2018
Editor: D. Vance

Keywords:
tree ring
oxygen isotope
Himalaya
ice core
South Asian Summer Monsoon
westerlies

ABSTRACT

Oxygen isotope ratios ($\delta^{18}O$) are the most commonly used parameters recorded in paleoclimate archives since they link different natural archives via the water cycle. Tree-ring $\delta^{18}O$ ($\delta^{18}O_{TR}$) has been widely used for hydroclimate reconstructions in the Himalaya. However, few of them record temperature signals, which are dominant in Himalaya ice-core $\delta^{18}O$. We hypothesize that the "precipitation amount effect" due to the South Asian Summer Monsoon (SASM) may overprint temperature signals in $\delta^{18}O_{TR}$ series. The purpose of this study is to investigate whether temperature signals could be found in the $\delta^{18}O_{TR}$ in locations where the influence of SASM is weak. We developed a 105-yr $\delta^{18}O_{TR}$ chronology from the northern slope of the western Himalaya which greatly blocks the SASM. Our $\delta^{18}O_{TR}$ clearly shows stronger correlations with temperature (dominant winter and weak summer) than summer precipitation signals. It also agrees well with summer soil moisture $\delta^{18}O$ simulated by the global isotope model LMDZ4 ($r = 0.72$, 1979–2010). In LMDZ4, low winter temperature was found to increase winter snowfall and subsequent snow melt, and thus to increase the contribution of winter snowfall to soil moisture in summer at the expense of summer precipitation. Since winter snowfall is more depleted than summer precipitation, this leads to lower summer soil moisture $\delta^{18}O$. The temperature signals found in our $\delta^{18}O_{TR}$ series are consistent with those found in the Dasuopu ice-core $\delta^{18}O$. This implies that $\delta^{18}O_{TR}$ series from the southwest Tibetan Plateau (TP), with a weak monsoon, hold great potential to capture temperature signals. Climate interpretations of $\delta^{18}O$ proxies in the Himalaya largely depend on the influence of seasonal water from the dominant atmosphere circulation systems of the westerlies or monsoon. The $\delta^{18}O$ proxies from the monsoon-affected region have a higher potential for the reconstruction of boreal summer hydroclimate, whereas $\delta^{18}O$ proxies from westerly-affected sites have a higher potential for temperature reconstructions.

1. Introduction

The Himalaya are a target area of global paleoclimate research due to their sensitivity to climate change and a variety of climate proxies such as tree rings (Sano et al., 2017; Xu et al., 2018) and ice cores (Thompson et al., 2000; Tian et al., 2012; Zhao et al., 2017). These proxies offer valuable climate information from areas with comparatively low anthropogenic disturbances. Oxygen isotope ratios ($\delta^{18}O$) are one of the most commonly used parameters in paleoclimate research, since the precipitation source-water $\delta^{18}O$ signal during incorporation and storage into the climatic archive is influenced by climatic factors (McCarroll and Loader, 2004; Thompson et al., 2018; Yao et al., 2013; Yu et al., 2016a, 2016b; Zeng et al., 2016). However, identification of the influence of specific climate signals in $\delta^{18}O$ series from different proxies is essential.

* Corresponding author at: Key Laboratory of Alpine Ecology, Institute of Tibetan Plateau Research, Chinese Academy of Sciences, Beijing 100101, China.
E-mail address: zhuhf@itpcas.ac.cn (H. Zhu).

https://doi.org/10.1016/j.epsl.2018.11.002
0012-821X/

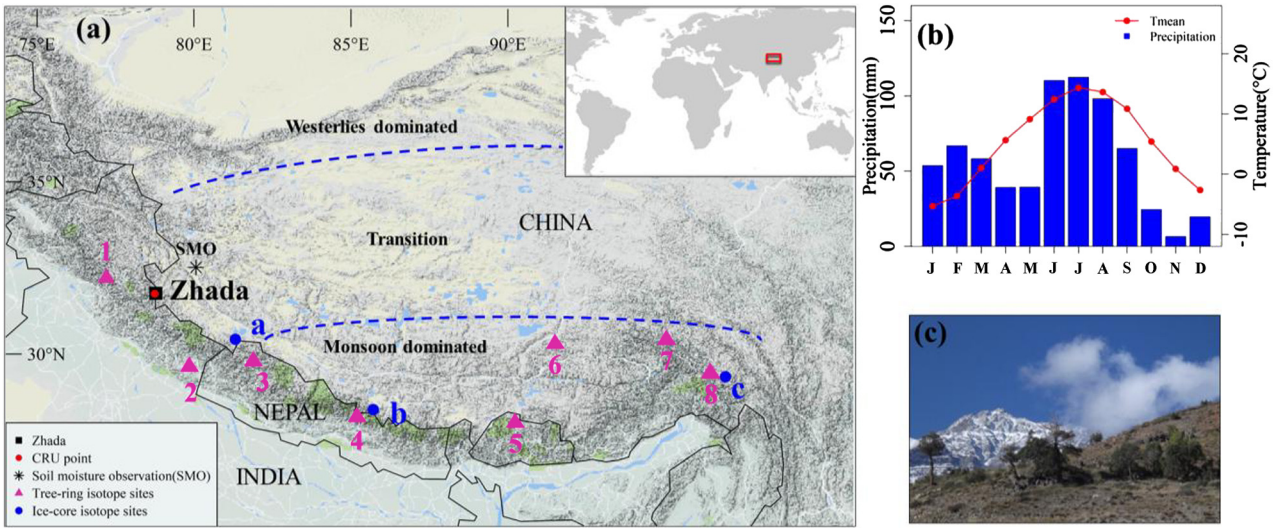

Fig. 1. (a) Locations of the Zhada sampling site in the southwest TP, the CRU grid point, nearest soil moisture observation (SMO) and nearby $\delta^{18}O_{TR}$ sites: 1 – western Himalaya, northwest India (Manali) (Sano et al., 2017), 2 – western Himalaya, north India (Jageshwar) (Xu et al., 2018), 3 – central Himalaya, western Nepal (Humla) (Sano et al., 2011), 4 – central Himalaya, central Nepal (Ganesh) (Xu et al., 2018); 5 – Bhutan Himalaya (Sano et al., 2013); 6 – Reting (Grießinger et al. 2011); 7 – Xinpu (Wernicke et al., 2017); 8 – Ranwu (Liu et al., 2014). Sites 7–8 belong to the eastern Himalayan range. The $\delta^{18}O_{IC}$ sites: a – Naimona'nyi (Tian et al., 2012); b – Dasuopu (Thompson et al., 2000); c – Zuoqiupu (Zhao et al., 2017). (b) Monthly climate variables from the CRU (TS3.24.01, 1979–2015, temperature) and TRMM (3B43_month, 1998–2015, precipitation). (c) Forest relicts at our sampling site. The topographical background is from https://www.google.com/maps. Based on Yao et al. (2013) and Thompson et al. (2018), three major climate regimes are proposed over the TP: monsoon-dominated region, westerlies-dominated region, and their transitional regions. The dashed lines denote the schematic boundaries separating the three climate regimes. (For interpretation of the colors in the figure(s), the reader is referred to the web version of this article.)

$\delta^{18}O$ variations in tree-ring cellulose (in the following $\delta^{18}O_{TR}$) from study sites located in regions affected by the South Asian Summer Monsoon (SASM) are strongly influenced by precipitation (Grießinger et al., 2011; Sano et al., 2013; Xu et al., 2018), relative humidity (Grießinger et al., 2017; Wernicke et al., 2017), cloud cover (Liu et al., 2014), and thus can also be linked to drought indices like the Palmer Drought Severity Index (PDSI) (Sano et al., 2011, 2017) (Fig. 1a). In most ice-core $\delta^{18}O$ ($\delta^{18}O_{IC}$) records from the Himalaya (Fig. 1a), however, temperature signals dominate isotope variability (Thompson et al., 2000; Tian et al., 2012; Zhao et al., 2017). These discrepancies in climate signals between tree-ring and ice core proxies raise the question: why is there no dominant temperature signal in the $\delta^{18}O_{TR}$ series from the SASM region, which is currently the most available and accurately dated proxy?

The identification of moisture sources of precipitation $\delta^{18}O$ ($\delta^{18}O_P$) may help to explain the missing temperature signal in $\delta^{18}O_{TR}$. The Himalaya are mainly influenced by two atmospheric circulation systems: SASM and mid-latitude Westerlies. The SASM introduces moist air masses to the southern slopes of the Himalaya during the summer season (May–September). Although some north–south steep valleys serve as SASM moisture transport corridors, the intensity and duration of SASM-derived rainfall is strongly reduced in the rain shadow in the northern Himalaya (Yu et al., 2016a). The mid-latitude Westerlies directly influence winter precipitation regime and summer mid-to high tropospheric dynamics (Mölg et al., 2014). $\delta^{18}O_p$ originating from the South Asian Monsoon region mainly responds to an "amount effect" since strong monsoon activity leads to high precipitation rates and depletes the heavy isotopes by fractionation processes (Tian et al., 2003; Yao et al., 2013). In contrast, isotope fractionation in precipitation derived from the westerlies is largely influenced by temperature effects, as temperature determines the condensation of precipitation formation (Tian et al., 2003; Yao et al., 2013). Accordingly, we hypothesize that the influence of the SASM may overprint temperature signals in $\delta^{18}O_{TR}$ series in the SASM region during the summer monsoon season (Fig. 1a).

The aim of this study is to test whether temperature signals could be recorded by $\delta^{18}O_{TR}$ series from the northern slope of the Himalaya where the SASM is blocked by the topography. We developed the first tree-ring $\delta^{18}O$ record for this area and investigated its climate signals with CRU observations, and a simulation with an isotope-enabled general circulation model (LMDZ4). This study helps to interpret and disentangle the climatic signals contained in $\delta^{18}O$ series from this climatologically complex region, and to design suitable sampling strategies for further paleoclimate reconstructions.

2. Materials and methods

2.1. Study area and its ecohydrological characteristics

Our study area is located on the northern slope of the western Himalaya, on the southwestern Tibetan Plateau (TP), China (Fig. 1a). As shown by the nearest CRU and Tropical Rainfall Measuring Mission (TRMM) grid data (CRU TS 3.24.01, 1979–2015, Fig. 1b; TRMM, 3B43_Month, 1998–2015) (Harris et al., 2014; Huffman et al., 2007), annual precipitation is around 694 mm, with 61.24%/38.76% of it falling during the summer (May–September)/winter seasons (October–April). This results in a characteristically bimodal distribution with two precipitation maxima in winter (from January to March) and summer (from June to August) (Fig. 1b). The coldest and warmest months are January (−5.3 °C) and July (14.4 °C), respectively.

Characterized by the semi-arid environment of the southwestern Tibetan Plateau, the Zhada sampling site (Fig. 1a, 78.78°E, 31.77°N, 2900–3700 m a.s.l.) is a relict forest stand composed of around 40 *Juniperus semiglobosa* trees lying in the rain shadow of the Himalaya. Like most juniper species in High Asia (Miehe et al., 2008), the junipers here grow on the south-facing slopes of a valley with weathered bedrock. It is characterized by dry, shallow and well-drained soils on a steep slope (30°∼40°) (Fig. 1c). Due to the semi-arid environment, species richness is extremely low and plants at the sampling site mainly including *Juncus* spp. and *Caragana* spp. (Fig. 1c). Under such a harsh environment, the juniper

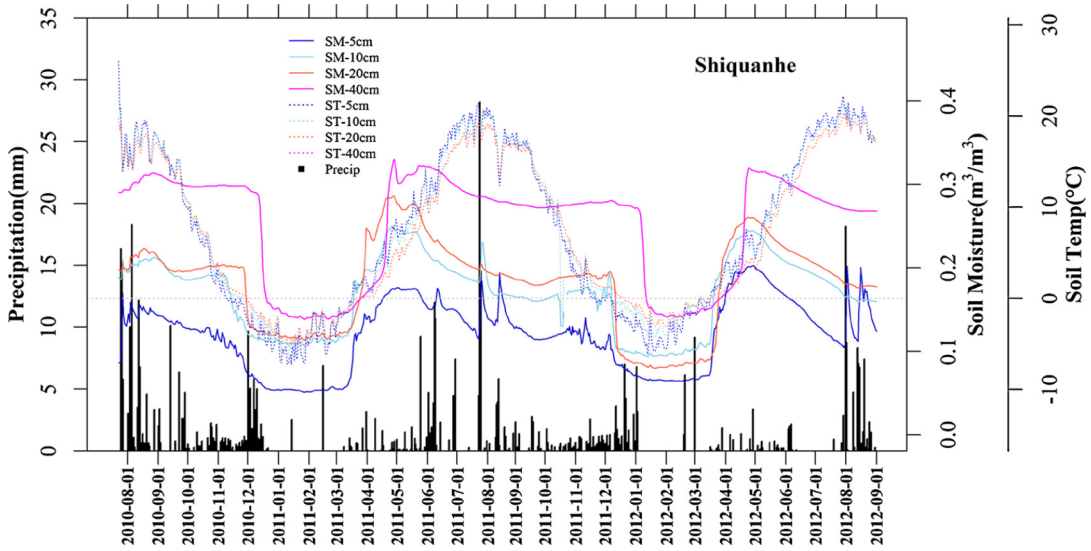

Fig. 2. Soil moisture and temperature observations from four depths (5 cm: medium blue, 10 cm: sky blue, 20 cm: tomato, 40 cm: magenta, 2010/7/23–2012/09/02, 130 km from our Zhada sampling site, Su et al., 2011) and the corresponding daily precipitation from TRMM (3B42_daily) in Shiquanhe (Fig. 1a, SMO). SM, ST, Precip stands for soil moisture, soil temperature, precipitation amount, respectively. The horizonal dotted lines indicate the soil temperature at 0 °C.

root systems reach a depth of more than 40 cm below ground following the precipitation infiltration depth (Miehe et al., 2008; Fan et al., 2017).

As observed in our study area (Fig. 2, Su et al., 2011), temperatures below 0 °C and the influence of the Westerlies lead to snow fall during the winter period (e.g. end of Nov. till end of Mar. next year). From the end of March to the beginning of April, snow starts to melt and replenishes the soil moisture at the 5 cm, 10 cm, 20 cm and 40 cm levels below surface. The snowmelt-induced soil moisture increase at 40 cm is not influenced by the summer monsoon (Fig. 2, Su et al., 2011). As such, the root-zone soil moisture is largely replenished from the winter snowmelt, and the influence of summer monsoon rainfall on root zone soil moisture is limited. Additionally, soil moisture is much higher in the deep soil level (10 cm, 20 cm, 40 cm) than in the surface soil (5 cm, Fig. 2), matching the depths of juniper root systems and their hydrotropism.

2.2. Tree-ring sampling and cellulose oxygen isotope measurement

During a field campaign in September 2015, 102 cores from 32 trees were collected. Subsequently, annual tree-ring widths were measured using a Lintab 5 system (®Rinntech, Heidelberg, Germany). The individual tree-ring series were cross-dated using dendrochronological procedures. We selected five cores from five trees for further $\delta^{18}O_{TR}$ analysis, based on the following criteria: (1) avoidance of missing rings, (2) sufficient amounts of material, (3) clearly detectable tree-ring boundaries. Annual rings were separated with a scalpel and treated individually following the procedures of α-cellulose extraction (Grießinger et al., 2017). Afterwards, cellulose homogenization was performed followed by freeze-drying (Grießinger et al., 2017).

The oxygen isotopes ratios of all tree-ring samples were determined using a Delta V Advantage Isotope Ratio Mass Spectrometer (Thermo Fischer Scientific Inc.) with a HEKAtech pyrolysis reactor in the tree-ring laboratory of the Institute of Geography at University of Erlangen-Nürnberg, Germany. All measurements are expressed as per mil deviations from IAEA 601/602 standards. The precision of the oxygen isotope measurement was 0.2‰. We found no age-related trends in the individual $\delta^{18}O$ series (Fig. S1), as reported in some earlier studies (Shi et al., 2011). Furthermore, the individual isotope chronologies were averaged into a standard chronology, and its reliability was tested with Rbar, Expressed Population Signal (EPS) and Gleichläufigkeit (GLK). Rbar is the mean inter-tree correlations, and is employed to compute the EPS to assess how well the final chronology with limited replication is represented in the constructed chronology. Additionally, GLK is a classical agreement parameter based on sign tests, indicating the coherence among series.

2.3. Modeling climate and isotope ratios in source water

The LMDZ4 is a General Circulation Model (GCM) developed at the Laboratoire de Météorologie Dynamique (LMD) (Hourdin et al., 2006). It is enabled with water stable isotopes (LMDZ-iso, Risi et al., 2010). When used in stand-alone mode, its land surface is represented by a simple bucket, which collects the soil water. The composition of this bucket is used here ($\delta^{18}O_{SW}$). No fractionation is considered during bare soil evaporation or leaf transpiration, although these processes can significantly impact the isotopic composition of soil moisture and plant tissues (Risi et al., 2016). However, as will be shown in the following, even without accounting for these processes, the simple bucket isotopic composition is able to capture the observed $\delta^{18}O_{TR}$ surprisingly well. Oxygen isotopes simulated by LMDZ4 have been widely used to compare with observations of $\delta^{18}O$ in precipitation ($\delta^{18}O_P$, Yao et al., 2013), ice cores ($\delta^{18}O_{IC}$, Yu et al., 2016b), and tree ring cellulose ($\delta^{18}O_{TR}$, Shi et al., 2011) over the TP.

The LMDZ4 simulation used here is described in detail in Risi et al. (2010). It is archived as part of the SWING2 (Stable Water INtercomparison Group phase 2) project. The spatial resolution is 3.75° in longitude ×2.5° in latitude. The simulation covers the 1979–2010 period after a 2-yr spinup. The sea surface conditions are prescribed following the AMIP (Atmospheric Model Intercomparison Project) protocol (Gates, 1992). To ensure that the meteorological situations of each year are correctly reproduced by LMDZ4, the horizontal winds are nudged (Yoshimura et al., 2008; Risi et al., 2010) towards those of the ERA-40 reanalyses (Uppala et al., 2005). The isotopic simulation is evaluated in the supplementary materials. To reveal the climate factors influencing the Zhada $\delta^{18}O_{TR}$, monthly outputs of precipitation and temperature as well as $\delta^{18}O$ in precipitation ($\delta^{18}O_P$) and in soil moisture ($\delta^{18}O_{SW}$) were analyzed. Values for Zhada are extracted from the nearest grid point.

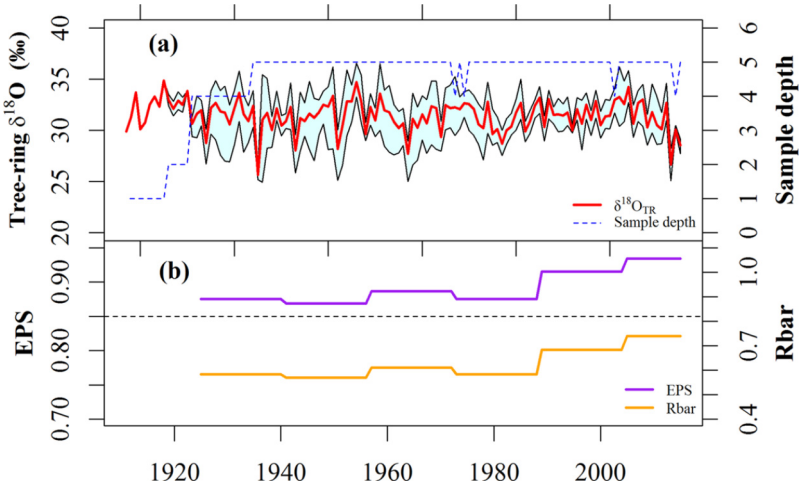

Fig. 3. (a) Zhada average $\delta^{18}O_{TR}$ chronology (red line) from five trees and the corresponding sample depth (blue dotted line). The light cyan shadow indicates the difference between minimum and maximum $\delta^{18}O$ values for the individual series. (b) Running EPS and Rbar values are calculated over 30 years lagged by 15 years, and the black dotted line indicates the EPS threshold value of 0.85.

2.4. Investigation of climate signals in Zhada $\delta^{18}O_{TR}$ series

We performed Pearson's correlations between the Zhada $\delta^{18}O_{TR}$ and temperature and precipitation of the grid point nearest to our sampling site from the CRU ($0.5° \times 0.5°$, 1979–2015) (Harris et al., 2014), and from the LMDZ4 simulation. To further test spatial relationships of our $\delta^{18}O_{TR}$ chronology, correlation fields between climate variables from the two datasets (CRU and LMDZ4) and the Zhada $\delta^{18}O_{TR}$ were created using the KNMI climate explorer (http://climexp.knmi.nl/).

2.5. Mechanisms analysis of summer soil $\delta^{18}O$ variability in the LMDZ4

To investigate the mechanisms controlling summer soil $\delta^{18}O$ variability in LMDZ4, we reconstructed the monthly snow and soil budget from monthly outputs. Specifically, we calculated the snow and rain precipitation, snow and soil evaporation, snow melt and soil runoff, based on equations detailed in the supplementary material. The reconstructed summer soil moisture and summer soil moisture $\delta^{18}O$ significantly correlated with those directly simulated by LMDZ4, with $r = 0.67$ ($p < 0.01$) and $r = 0.41$ ($p < 0.05$), respectively. Then, the summer soil moisture $\delta^{18}O$ of each year from 1979 to 2010 was decomposed into contributions from snow melt, rainfall and runoff from the different months. The contribution of these different effects to the yearly variability in summer soil moisture $\delta^{18}O$ was finally estimated by calculating the regression coefficients between summer soil moisture $\delta^{18}O$ and the effects of each process, as detailed in the supplementary material. This analysis was complemented with the calculation of correlations between climate signals identified statistically with the tree-ring $\delta^{18}O$ and process-related variables from LMDZ4.

2.6. Lagrangian moisture source diagnostic for Zhada sampling site

To detect moisture contributions to the Zhada sampling site during winter (February–March) and summer (June–July–August), moisture sources were diagnosed from a 34-yr climatology of air mass transport (Läderach and Sodemann, 2016). The climatology has been calculated with the Lagrangian transport model FLEXPART (Stohl et al., 2005) using the ERA-Interim reanalysis dataset covering the period 1980–2013 (Dee et al., 2011). Moisture sources were identified along 10-day air mass back trajectories arriving in the target region (78.5–80°E, 31–33°N) with a relative humidity larger than 70%, using the method of Sodemann et al. (2008). Locations along the airmass trajectories where specific humidity increased by more than 0.1 g kg^{-1} in a 6 h time interval forward in time were considered as moisture sources. No distinction was at this point made between boundary-layer sources and sources in the free troposphere. Periods of specific humidity decrease were considered as precipitation events, weighted by their fractional contribution to the moisture already present in air parcels, and the contribution of previous source regions were reduced accordingly. This yields a quantitative estimate of the contribution of evaporation at the moisture sources to precipitation in the target region.

3. Results

3.1. Tree-ring $\delta^{18}O$ series

The lengths of the individual $\delta^{18}O_{TR}$ series were 92, 105, 119, 105, and 110 years, respectively. The reliability of the mean chronology, as measured by the expressed population signal (EPS) statistic, passed the recommended threshold of 0.85 (Fig. 3). In addition, the individual $\delta^{18}O_{TR}$ series showed high synchronicity (Fig. 3a), as revealed by a mean GLK of 0.63 and an overall mean EPS of 0.88. The chronology period 1911–2015 was selected for further comparisons, as the sample depth was continuously higher than four individuals after AD 1911. Over the period from 1911 to 2015, the range of Rbar and EPS between the five trees calculated for 30-yr windows with a 15-yr overlap ranged from 0.58–0.74 (Rbar) and 0.87–0.93 (EPS), documenting a strong common forcing among the five individual isotope series and confirming the robustness of our mean $\delta^{18}O$ chronology.

3.2. Relationship between the Zhada $\delta^{18}O_{TR}$ and climate variables

Generally, the Zhada $\delta^{18}O_{TR}$ shows highest correlations with temperature (Fig. 4). Compared to the correlations with other individual months, the correlation with CRU February mean temperature is relatively high. The highest correlation with LMDZ4 temperature is found for seasonal means from February to March (Tmean(2–3), $r = 0.63$, $p < 0.01$, df $= 29$) and June to August (Tmean(6–8), $r = 0.50$, $p < 0.01$, df $= 29$, Fig. 6 and Fig. S2). Spatially, it shows significant correlations ($p < 0.05$) with CRU and LMDZ4 temperatures averaged from February to March over the southwestern TP and regions to the northwest and southwest (Fig. 5). Although the spatial extension of correlations with summer temperature (June–August) is regionally limited, these results

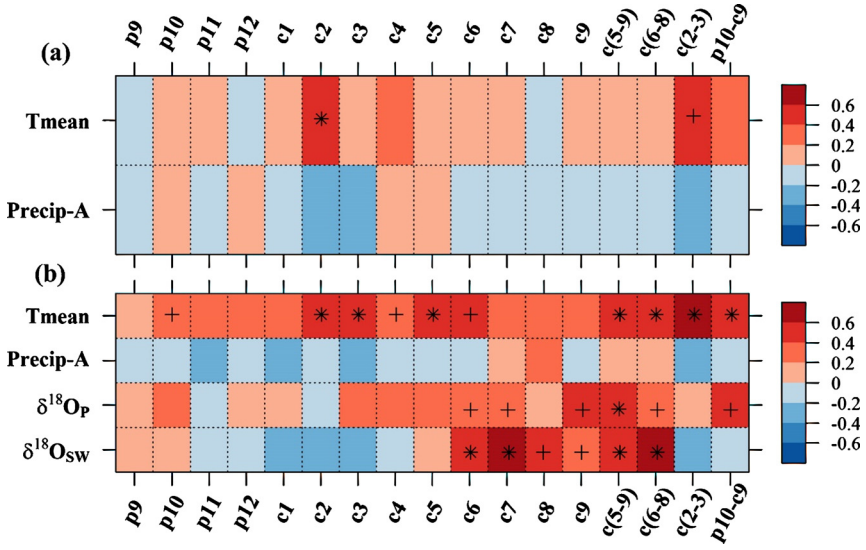

Fig. 4. Correlations between the Zhada $\delta^{18}O_{TR}$ and monthly variables from the (a) CRU TS3.24.01 (1979–2015) and (b) LMDZ4 (1980–2010) data sets. Y-axes: Tmean, Precip-A, $\delta^{18}O_P$, $\delta^{18}O_{SW}$ denote the monthly mean temperature, precipitation amount, monthly precipitation $\delta^{18}O$, and soil moisture $\delta^{18}O$, and respectively. X-axes: Numbers represent months and seasons of the current 'c' and previous 'p' years. The symbols '+' and '∗' indicate the significance levels at $p < 0.05$ and $p < 0.01$, respectively.

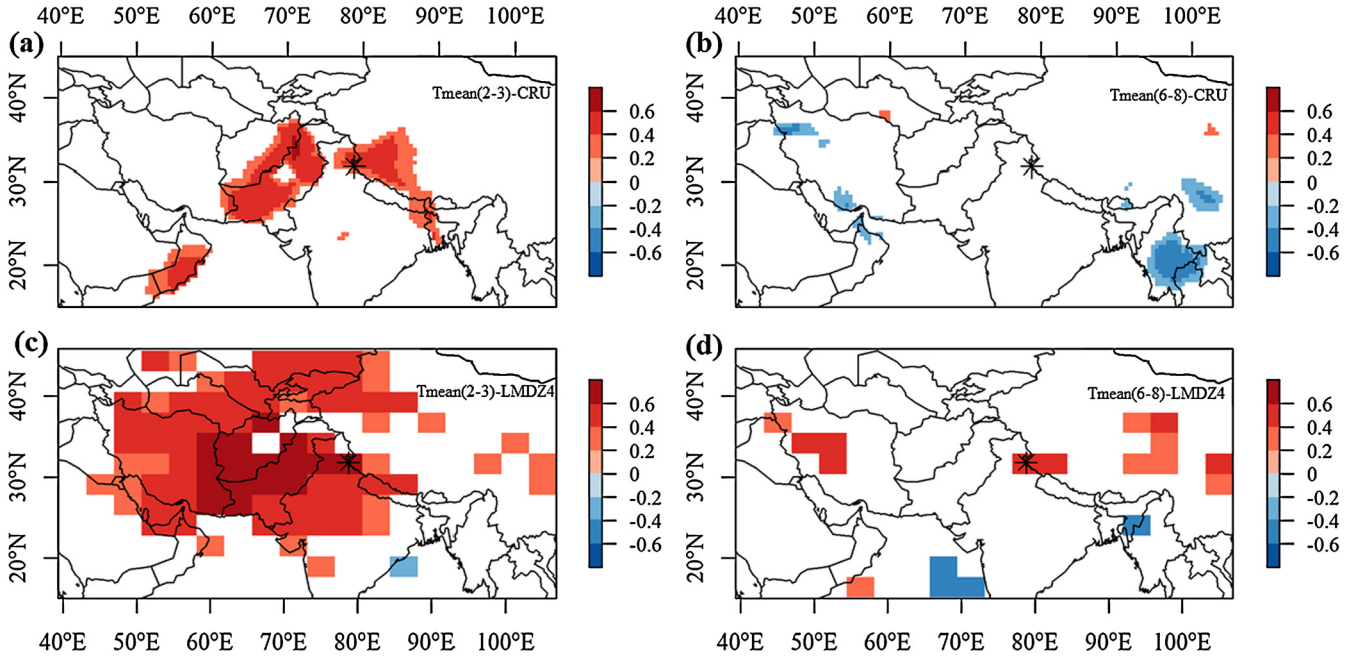

Fig. 5. Spatial correlations between Zhada $\delta^{18}O_{TR}$ series and mean temperatures (CRU TS 3.24.1, LMDZ4) during winter (February and March, Tmean(2–3)) and summer (June–July–August, Tmean(6–8)). (a) CRU data, 1979–2015, Tmean(2–3); (b) CRU data, 1979–2015, Tmean(6–8); (c) LMDZ4 data, 1979–2010, Tmean(2–3); (d) LMDZ4 data, 1979–2010, Tmean(6–8). The black asterisk indicates the location of our sampling site. Only correlations significant at $p < 0.05$ are displayed.

strongly indicate the signals of Tmean(6–8) and Tmean(2–3) in our Zhada $\delta^{18}O_{TR}$ series (Fig. 5). Moreover, the spatial correlations with variables (LMDZ4) during winter and summer periods (Fig. S3 and Fig. S4) show significant and spatially robust relationships between temperature and Zhada $\delta^{18}O_{TR}$. Furthermore, correlations between Zhada $\delta^{18}O_{TR}$ and LMDZ4 Tmean(2–3) stay significant when excluding the effect of Tmean(6–8) ($r = 0.51$, $p < 0.01$), while relationship between Zhada $\delta^{18}O_{TR}$ and LMDZ4 Tmean(6–8) turns insignificant when excluding the influence of Tmean(2–3) ($r = 0.26$, $p > 0.05$). These partial correlations further suggest the robustness of winter temperature signals in the Zhada $\delta^{18}O_{TR}$.

In addition, the Zhada $\delta^{18}O_{TR}$ shows significant correlations with LMDZ4 modeled summer soil moisture oxygen isotopes ($\delta^{18}O_{SW}$, June–August) (Fig. 4b, $r = 0.72$, $p < 0.01$, df $= 29$). Their inter-annual variations display a clear coherence for both the raw and first-differenced data (Fig. 6a and Fig. S2a). The averages of $\delta^{18}O_{SW}$ and $\delta^{18}O_{TR}$ during the period 1979–2010 are −3.38‰ and 31.44‰, respectively, implying that on average ∼34.8‰ isotopic enrichment occurred during the whole fractionation path from source water to tree-ring cellulose. This value lies within the postulated range of $\delta^{18}O_{TR}$ enrichment up to 47‰ as mentioned by McCarroll and Loader (2004).

3.3. Mechanisms linking summer soil moisture $\delta^{18}O$ variability with climate variables in the LMDZ4

As presented in Table 1, processes in May contribute the highest proportion (72.46%) to soil moisture $\delta^{18}O$ variability. In contrast, processes in summer (June–August) only contribute 35.77%, with half of this in June (17.37%). Accordingly, we hypothesize

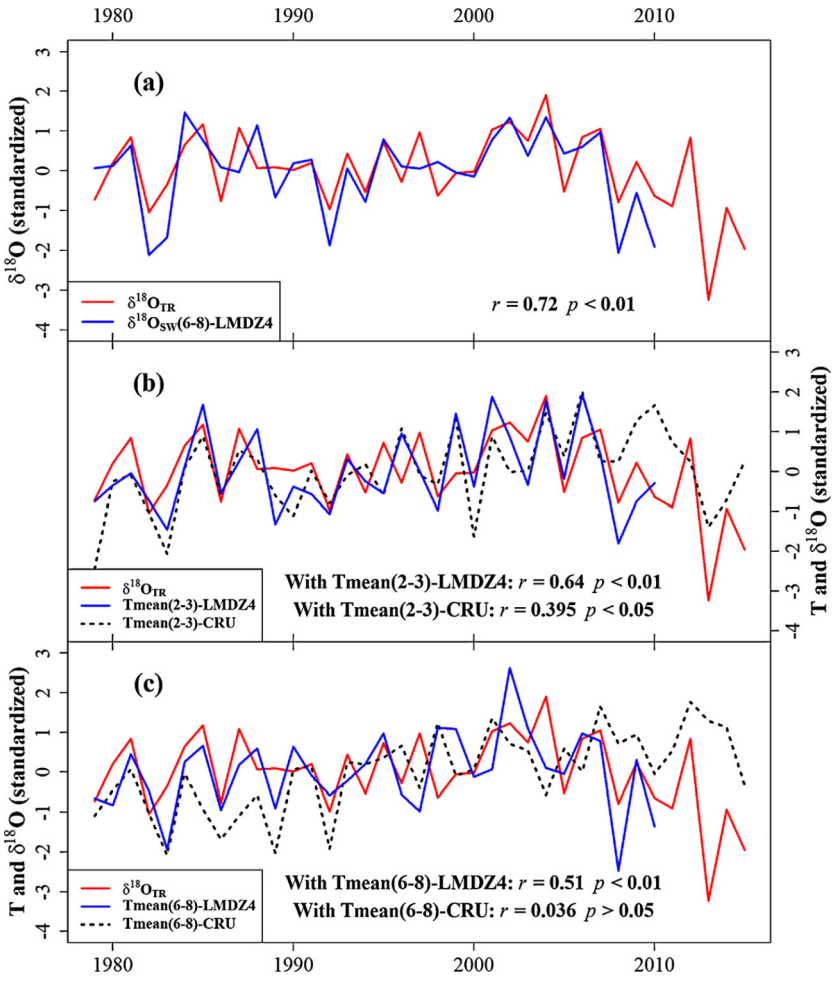

Fig. 6. Comparison between the Zhada $\delta^{18}O_{TR}$ and variables from CRU TS3.24.01 (1979–2015), LMDZ4 modeling (1979–2010) for the raw data. (a) with soil moisture oxygen isotopes averaged from current June to August ($\delta^{18}O_{SW}$(6–8)); (b) with Tmean(2–3); (c) with Tmean(6–8).

Table 1
Contribution of snowmelt, rainfall, runoff to the variability of summer soil moisture $\delta^{18}O$.

Month	Snowmelt	Rainfall	Runoff	Monthly sum	Seasonal sum
April	−11.95%	1.51%	2.37%	−8.06%	64.40%
May	22.64%	26.98%	22.84%	72.46%	
June	/	8.13%	9.24%	17.37%	35.77%
July	/	−10.36%	14.67%	4.30%	
August	/	6.15%	7.96%	14.10%	
Process sum	10.70%	32.40%	57.07%	/	/

that winter temperature signals may be transferred through snow-related processes (snowfall and subsequent snowmelt) in May, soil moisture in May then to summer soil moisture $\delta^{18}O$. In addition, overall, runoff is the major contribution to summer soil moisture $\delta^{18}O$ (Table 1). Runoff does not fractionate. Rather, it has an impact on the relative proportion of precipitation and snow melt from the different seasons. Runoff regulates the contribution of snow melt, which comes from depleted winter precipitation, and of summer rain fall, which is enriched, to summer soil moisture.

Fig. 7 presents the final tested significant relationships between winter temperature and summer soil moisture $\delta^{18}O$ record. It can be identified that lower temperature is related to more snowfall in winter ($r = -0.4$, $p < 0.05$) and greater spring snow depth ($r = -0.66$, $p < 0.01$). Greater snow depth in spring provides more water from snowmelt ($r = 0.86$, $p < 0.01$). This fills the soil, whose maximum capacity is 150 mm in LMDZ4 (Risi et al., 2010). June precipitation, which is more enriched, thus has more difficulty to infiltrate in the soil moisture. Therefore, the contribution of enriched summer rainfall to summer soil moisture is lower, and the soil moisture $\delta^{18}O$ is more depleted.

3.4. Moisture source diagnostic for the Zhada sampling site during winter and summer

Fig. 8 demarcates the moisture sources for the Zhada site during 1980–2013. The main moisture sources were, for the winter season, identified in the southwestern parts of the Tibetan Plateau (inner stippled contours, Fig. 8a), mainly northwest India and southern Pakistan. The main summer moisture sources were identified as local, with 50% originating within a range of 300–400 km (inner stippled contours, Fig. 8b). The percentage contribution from the Indian Ocean (monsoon) in summer is very limited.

4. Discussion

4.1. Temperature signals in the Zhada $\delta^{18}O_{TR}$ series

Two major processes could cause the Zhada $\delta^{18}O_{TR}$ chronology to be controlled by temperature. One is via summer soil moisture $\delta^{18}O_{SW}$ (source water), the other is the physiological fractionation from source water to tree-ring cellulose due to leaf enrichment (McCarroll and Loader, 2004). As partial correlations between $\delta^{18}O_{TR}$ and summer $\delta^{18}O_{SW}$ ($r = 0.6$, $p < 0.01$) or Tmean(2–3)

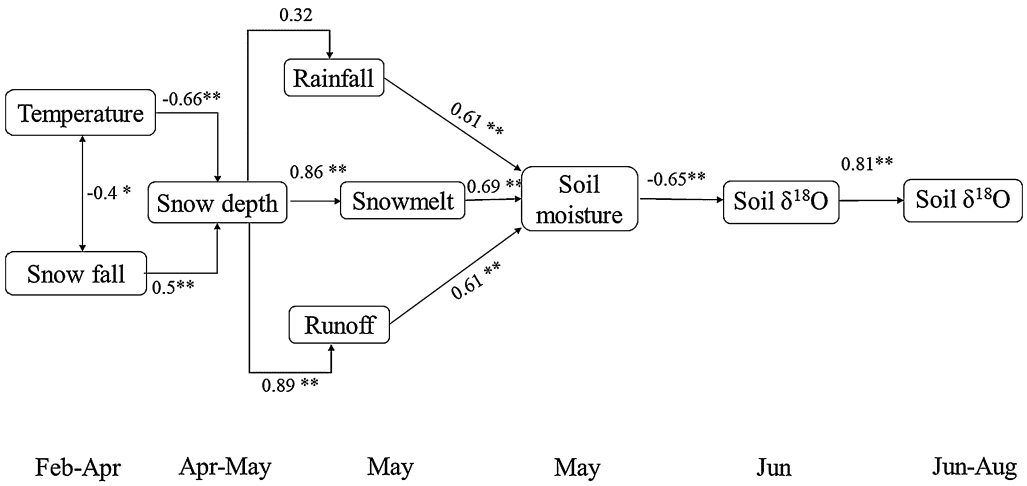

Fig. 7. Flow chart illustrating the linkage of winter temperature with soil $\delta^{18}O$. The text at the bottom shows the months for the variables above. Arrows indicate the relationships among variables. Numbers between two variables stand for their correlations. Correlations at 95%, 99% significant level are marked with one asterisk, two asterisks, respectively.

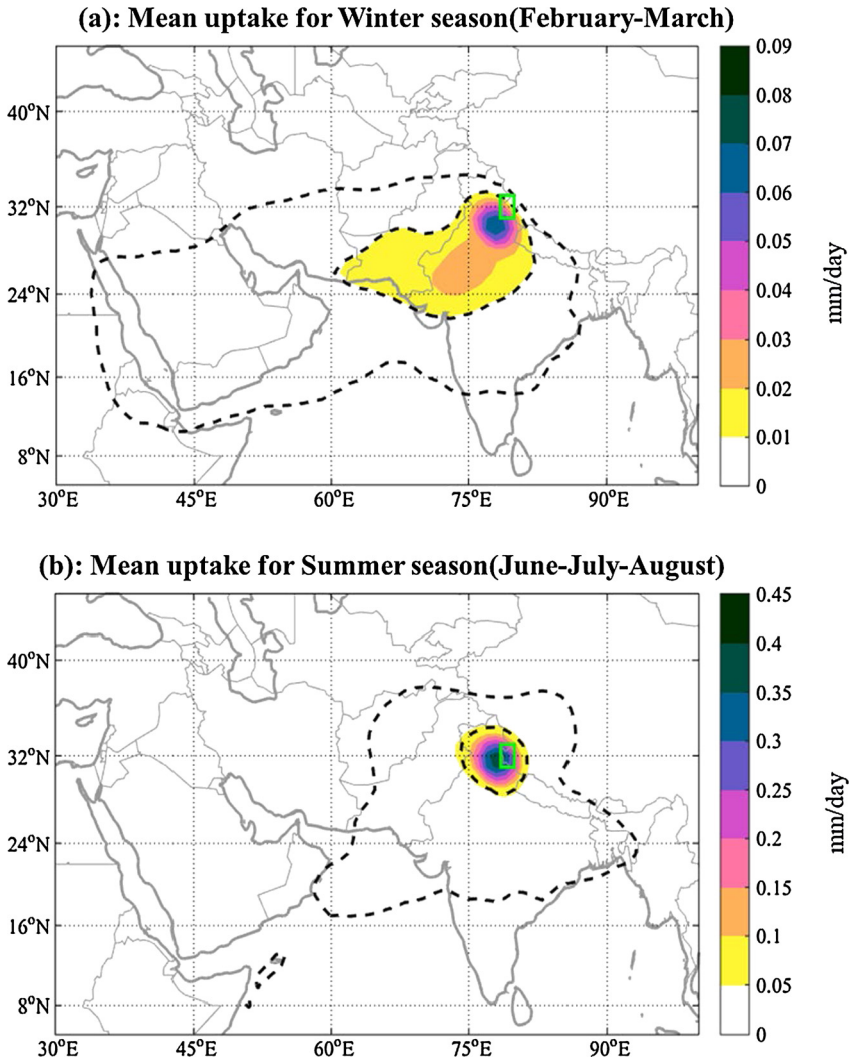

Fig. 8. Seasonal mean moisture source regions for the Zhada sampling site (78.5–80°E, 313-3°N), extracted from the 1980–2013 ERA-Interim reanalysis data using a Lagrangian moisture source diagnostic. Note the different scales. Color shows the contribution of local evaporation to precipitation in the target region (mm day^{-1}). Stippled contours show the 50th (inner) and 90th (outer) percentiles of the accumulated moisture source distribution. (a) Winter season (February–March); (b) summer season (June–July–August).

($r = 0.51$, $p < 0.01$) stay significant when excluding the effect of Tmean(6–8), it can be inferred that most of the temperature signal is transferred to tree-ring cellulose through the summer $\delta^{18}O_{SW}$ (source water) rather than through physiological process.

4.2. Possible transfer of the winter temperature signal into summer soil moisture

The winter temperature signals would be propagated into summer $\delta^{18}O_{SW}$ via two steps: fractionation during snow formation followed by isotope fractionation processes after snowfall (sublimation, evaporation, snowpack melting, refreezing). During snow formation, the value of $\delta^{18}O_P$ is lower in colder conditions because the vapor becomes more depleted as the Rayleigh distillation proceeds (McCarroll and Loader, 2004; Tian et al., 2003). However, correlations between summer $\delta^{18}O_{SW}$ and winter precipitation $\delta^{18}O$ (February–March) ($r = 0.07$, $p > 0.05$) are weak. Therefore, processes rather than Rayleigh distillation relate winter temperature to summer $\delta^{18}O_{SW}$. In LMDZ4, as shown by our decomposition analysis (Fig. 7), winter temperature regulates the relative contribution of snow melt and of summer precipitation to the summer soil moisture: colder winters lead to a reduced contribution of enriched summer rainfall, which has more difficulty to infiltrate a soil that is already full of snow melt.

In nature, several lines of evidence collectively support the suggestion that winter snowmelt could contribute significantly to the source water for vegetation (including trees). Based on satellite observations and terrestrial process-based models, Wang et al. (2017) have detected that snowfall would contribute to the soil moisture used by vegetation in the Himalaya. Isotope-based empirical observations at the high elevations of North China (Zhang et al., 2018) and the arid mountainous area of western US (West et al., 2007) yield similar conclusions. Furthermore, our Zhada $\delta^{18}O_{TR}$ shows a clear resemblance to the Dasuopu $\delta^{18}O_{IC}$ record (Fig. 9), and the annual accumulation for Dasuopu ice-core dominantly originates from winter westerlies-transported snowfall (Pang et al., 2014), proving that winter snowmelt is the dominant water source for Zhada junipers.

4.3. Comparison with $\delta^{18}O_{TR}$ studies from monsoonal regions

Source water differences could explain the differing climate interpretations of Zhada and Manali $\delta^{18}O_{TR}$. The isotopic composition of the source water for trees largely depends upon the range of root depths from which the tree takes water up (Tang and Feng 2001). Average root depths of junipers are deeper than those of fir, as reported from a global synthesis for plant root depth (Fan et al., 2017). Therefore, junipers could mainly take up stored water from snowmelt under dry conditions (Fig. 1c), and the fir could mainly take up shallow water from summer rainfall under humid conditions (Sano et al., 2017). This could explain the different climate significances for Zhada $\delta^{18}O_{TR}$ (dominant winter and weak summer signals) from the North Himalaya and Manali $\delta^{18}O_{TR}$ from the South Himalaya (dominant summer and weak winter signals, Sano et al., 2017) (site 1 in Fig. 1a).

The temperature interpretation of Zhada $\delta^{18}O_{TR}$ also differs from the hydroclimate signals in other earlier published $\delta^{18}O_{TR}$ chronologies (Sites 2–8, Fig. 1). Extensive monsoon-transported rainfall would greatly overprint the $\delta^{18}O$-temperature relationship (Tian et al., 2003, Fig. S5 sites 1–8), and recharge the soil profile during the vegetation period, being the primary source water (Zeng et al., 2016). This could explain why the temperature signal doesn't dominate $\delta^{18}O_{TR}$ records from strongly SASM-affected regions (Fig. 1a).

4.4. Comparison with nearby ice-core $\delta^{18}O$ series

The temperature signal found in Zhada $\delta^{18}O_{TR}$ was similar to that from the Zuoqiupu $\delta^{18}O_{IC}$ (Zhao et al., 2017), in which the annual snow accumulation dominantly comes from westerlies-delivered precipitation during the non-monsoon season (October to May), though there is a considerable amount of summer monsoon-transported rainfall (Yang et al., 2013).

To further validate the temperature signals found in our $\delta^{18}O_{TR}$, we compared the Zhada $\delta^{18}O_{TR}$ with the independent temperature-dominated $\delta^{18}O_{IC}$ record from the Dasuopu glacier during 1911–1996 (Thompson et al., 2000). The Zhada $\delta^{18}O_{TR}$ shows a clear resemblance to the Dasuopu $\delta^{18}O_{IC}$ record for their 5-yr moving averaged data (Fig. 9a, 9b, $r = 0.32$, $p > 0.05$, df-adjusted $= 14.7$), especially before the 1960s. Both chronologies showed maxima during 1918–1922, 1945–1950 and minima during 1925–1935, 1957–1962, respectively, suggesting common climate signals. However, we cannot explain the existing mismatch after the 1960s, especially for the lower magnitude in 1970s in Zhada $\delta^{18}O_{TR}$ and 1980s in Dasuopu $\delta^{18}O_{IC}$.

We also employed the cross-dating technique commonly used in dendrochronology to test the similarity between both proxy series on inter-annual timescales. Over the whole common period, the two series are not significantly correlated ($r = 0.15$, df $= 84$, $p > 0.05$). However, there is a much better match between the chronologies during 1927–1963, if we shift the Dasuopu $\delta^{18}O_{IC}$ series one year back (Fig. 9c, 9d). Then the correlation between both records increased from 0.24 ($p > 0.05$) to 0.53 ($p < 0.01$). There is also correspondence between the two series in extreme years with minimum values in 1928, 1933, 1942, 1948 and 1957, similar to the pointer year approach in tree-ring crossdating. This coincidence suggests that $\delta^{18}O_{TR}$ and $\delta^{18}O_{IC}$ show consistent temperature signals at annual scale, and there is a possibility to perform cross-dating between the two proxies. Generally, either 1962 or 1963 was regarded as the base year to constrain the ice-core layer dating due to the relatively high beta radioactivity (Kehrwald et al., 2008). For the Dasuopu ice core, the base year for dating was 1963 (Thompson et al., 2000). Considering this highly significant correlation after shifting the ice core series for one year and the known precise dating of tree-rings, we suggest a modification of the ice core base year to 1962.

Moreover, the declining temperature trend during the recent ~15 years in the Zhada record has also been observed for nearby temperature-dominated ice-core $\delta^{18}O$ (Fig. S6, An et al., 2016; Thompson et al., 2018) as well as for regional meteorological observations (Fig. S7, CRU grid point, Shiquanhe and Burang). This further demonstrates the reliability of the Zhada $\delta^{18}O_{TR}$ as a temperature proxy. Considering the comparison with the meteorological observations and ice-core $\delta^{18}O$ series, the Zhada tree-ring $\delta^{18}O$ series mainly indicate temperature variations on annual to inter-decadal scales.

4.5. Comparison with other regional $\delta^{18}O$ proxies

At the regional scale, the intensity of monsoonal activity could largely determine the climatic significance of $\delta^{18}O_P$, which might explain the discrepant climate signals in different $\delta^{18}O$ proxies. So far, the current $\delta^{18}O_{TR}$ records over the southern TP are from inside the core monsoon zone, with a more pronounced monsoonal activity during the summer season (Sites 1–8, Fig. 1a and Fig. S5). Hence amount-affected precipitation $\delta^{18}O$ is mainly used for their wood synthesis during the vegetation period (Shi et al., 2011; Zeng et al., 2016). This results in a dominant hydroclimate signal and a suppression of temperature signals in these $\delta^{18}O_{TR}$ chronologies. At our Zhada

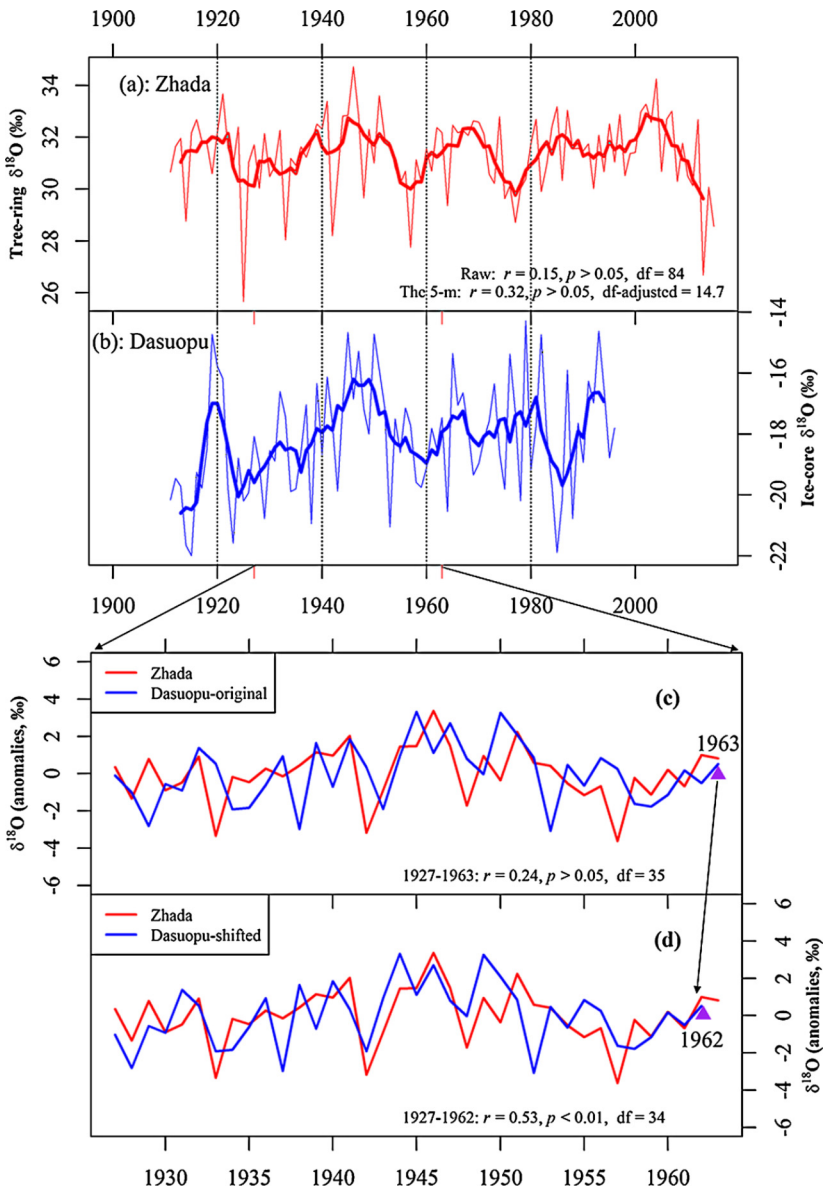

Fig. 9. Comparison between the Dasuopu $\delta^{18}O_{IC}$ (Thompson et al., 2000) and the Zhada $\delta^{18}O_{TR}$ during 1911–2015 (a and b) and 1927–1963 (c and d). The light and bold lines in (a) and (b) are the annual data and the 5-yr moving averages. The rationality of moving ice-cores $\delta^{18}O$ one year backward is discussed in the main text.

sampling site, the air parcels for the rainfall amount are dominantly transported by the westerlies during winter (Fig. 8a), and direct monsoon influence during summer appears to be too weak (Fig. 7b, Fig. S5, and Fig. 8b) to overprint the $\delta^{18}O$-temperature relationships. This could explain the dominant temperature signal found in our $\delta^{18}O_{TR}$. These findings are consistent with results from a $\delta^{18}O_{IC}$ record from the nearby westerlies-dominated Naimona'nyi glacier (Fig. 1a) (Tian et al., 2012). Thus, $\delta^{18}O$ proxies in monsoon and westerlies-influenced regions may record precipitation amount and temperature variations, respectively.

Such inferences could hold true even at the global scale. Precipitation-amount interpretations of $\delta^{18}O$ proxies are usually found in core monsoon-affected zones with extensive rainfall, like in the North American Monsoon region (Szejner et al., 2016), the South American Monsoon region (Brienen et al., 2012; Volland et al., 2016), the Asian Monsoon region (Grießinger et al., 2011; Sano et al., 2013), and the North African Monsoon region (van der Sleen et al., 2015). In contrast, temperature-dominated signals in $\delta^{18}O$ proxies occur in westerlies-dominated regions e.g., in northern Patagonia (Lavergne et al., 2016) and the southern Rocky Mountains (Berkelhammer and Stott, 2012). Consequently, sampling sites of $\delta^{18}O$ proxies in core monsoon regions would be preferred for boreal summer hydroclimate reconstructions, and sites in the westerlies-affected regions in northern and southern Hemispheres are more suitable for temperature reconstructions.

5. Conclusions

Aiming to test whether temperature signals could be found in the tree-ring oxygen isotope in the Himalaya, we built the first $\delta^{18}O_{TR}$ series from the northern slope of the Himalaya, southwestern TP, in which monsoon intensity is greatly reduced. Our $\delta^{18}O_{TR}$ is found to be more mediated by temperature (dominant winter and weak summer), rather than summer precipitation amount. Variability of our $\delta^{18}O_{TR}$ was well captured by the LDMZ4 summer soil moisture $\delta^{18}O$ ($r = 0.72$, 1979–2010). In LMDZ4, low winter temperature increases the contribution of winter snow to summer soil moisture at the expense of enriched summer precipitation.

The temperature effect of the Zhada $\delta^{18}O_{TR}$ series is further verified by consistency with nearby ice-core $\delta^{18}O$ variability. The lack of temperature signals from neighboring $\delta^{18}O_{TR}$ chronologies derived from summer monsoon-dominated regions may be related to the dominant amount effect that triggers $\delta^{18}O_P$ in the SASM region. Accordingly, to study temperature variability of the Himalaya or the Tibetan Plateau, we recommend oxygen isotope series from westerlies-dominated regions, rather than the SASM area.

Acknowledgements

We greatly acknowledge Editor Prof. Dr. Derek Vance and the anonymous reviewers for their critical comments and suggestions to substantially improve the manuscript. Editor Prof. Jess Adkins is also appreciated for his suggestions on the first version of the manuscript, although he was not responsible for it finally. This work was supported by the National Natural Science Foundation of China (41661144040 and 41571201, 41525001, 41671054), and the International Partnership Program of Chinese Academy of Sciences (131C11KYSB20160061). Haifeng Zhu is grateful for support from West Light Foundation of the Chinese Academy of Sciences. Ru Huang is grateful for the support from the UCAS Joint PhD Training Program (UCAS[2015]22). Harald Sodemann acknowledges the Swiss National Science Foundation for funding through grant No. 200021_143436 "Spatial and Temporal Scales of Linkages in the Atmospheric Water Cycle (Waterscales)". Thanks are given to Iris Burchardt, Roswitha Höfner-Stich (University of Erlangen-Nuremberg) for support during isotope analyses and Dr. Hans Christian Steen-Larsen (University of Copenhagen, Denmark), Dr. Jessica Baker (University of Leeds, UK), Dr. Tao Wang (ITPCAS), Dr. Jun Qin (ITPCAS) and Dr. Zeqing Ma (IGSNRR) for helpful suggestions on data analysis. We thank Dr. Shalik Sigdel (ITPCAS) for identifying the plant species, Dr. Chenxi Xu (IGGCAS) for providing the tree-ring oxygen isotope data in the South Himalaya. The oxygen isotope data of Dasuopu ice core is provided by the Third Pole Environment Database (http://www.tpedatabase.cn/). Tropical Rainfall Measuring Mission (TRMM) daily (Accessed [2017-1-10]) and monthly (Accessed [2017-05-08]) data are provided by the Goddard Earth Sciences Data and Information Services Center (GES DISC, daily: Precipitation L3 1 day 0.25 degree × 0.25 degree V7, https://disc.gsfc.nasa.gov/datacollection/TRMM_3B42_Daily_7.html; monthly: Rainfall Estimate L3 1 month 0.25 degree x 0.25 degree V7, https://disc.gsfc.nasa.gov/datacollection/TRMM_3B43_7.html). The LMDZ4 simulation was run thanks to high performance calculation resources of IDRIS under the allocation 0292 made by GENCI. It is archived as part of the SWING2 project and available at https://data.giss.nasa.gov/swing2/.

Appendix A. Supplementary material

Supplementary material related to this article can be found online at https://doi.org/10.1016/j.epsl.2018.11.002.

References

An, W., Hou, S., Zhang, W., Wu, S., Hao, X., Pang, H., Wang, Y., Liu, Y., 2016. Possible recent warming hiatus on the northwestern Tibetan plateau derived from ice core records. Sci. Rep. 6, 32813. https://doi.org/10.1038/srep32813.

Berkelhammer, M., Stott, L.D., 2012. Secular temperature trends for the southern Rocky Mountains over the last five centuries. Geophys. Res. Lett. 39 (17), L17701. https://doi.org/10.1029/2012gl052447.

Brienen, R.J., Helle, G., Pons, T.L., Guyot, J.L., Gloor, M., 2012. Oxygen isotopes in tree rings are a good proxy for Amazon precipitation and El Nino-Southern Oscillation variability. Proc. Natl. Acad. Sci. USA 109 (42), 16957–16962.

Dee, D.P., Uppala, S.M., Simmons, A.J., et al., 2011. The ERA-Interim reanalysis: configuration and performance of the data assimilation system. Q. J. R. Meteorol. Soc. 137, 553–597.

Fan, Y., Miguezmacho, G., Jobbágy, E.G., Jackson, R.B., Oterocasal, C., 2017. Hydrologic regulation of plant rooting depth. Proc. Natl. Acad. Sci. USA 114 (40), 10572–10577.

Gates, W.L., 1992. AMIP: the atmospheric model intercomparison project. Bull. Am. Meteorol. Soc. 73 (12), 1962–1970.

Grießinger, J., Bräuning, A., Helle, G., Thomas, A., Schleser, G., 2011. Late Holocene Asian summer monsoon variability reflected by $\delta^{18}O$ in tree-rings from Tibetan junipers. Geophys. Res. Lett. 38 (3), L03701. https://doi.org/10.1029/2010gl045988.

Grießinger, J., Helle, G., Hochreuther, P., Schleser, G.H., Bräuning, A., 2017. Late Holocene relative humidity history on the southeastern Tibetan plateau inferred from a tree-ring $\delta^{18}O$ record: recent decrease and conditions during the last 1,500 years. Quat. Int. 430, 52–59. https://doi.org/10.1016/j.quaint.2016.02.011.

Harris, I., Jones, P.D., Osborn, T.J., Lister, D.H., 2014. Updated high-resolution grids of monthly climatic observations-the CRU TS3.10 Dataset. Int. J. Climatol. 34 (3), 623–642.

Hourdin, F., Musat, I., Bony, S., et al., 2006. The LMDZ4 general circulation model: climate performance and sensitivity to parametrized physics with emphasis on tropical convection. Clim. Dyn. 27 (7–8), 787–813.

Huffman, G.J., Bolvin, D.T., Nelkin, E.J., et al., 2007. The TRMM multisatellite precipitation analysis (TMPA): quasi-global, multiyear, combined-sensor precipitation estimates at fine scales. J. Hydrometeorol. 8 (1), 38–55.

Kehrwald, N.M., Thompson, L.G., Yao, T., Mosley-Thompson, E., Schotterer, U., Alfimov, V., Beer, J., Eikenberg, J., Davis, M.E., 2008. Mass loss on Himalayan glacier endangers water resources. Geophys. Res. Lett. 35 (22), L22503. https://doi.org/10.1029/2008gl035556.

Läderach, A., Sodemann, H., 2016. A revised picture of the atmospheric moisture residence time. Geophys. Res. Lett. 43 (2), 924–933.

Lavergne, A., Daux, V., Villalba, R., Pierre, M., Stievenard, M., Vimeux, F., Srur A, M., 2016. Are the oxygen isotopic compositions of *Fitzroya cupressoides* and *Nothofagus pumilio* cellulose promising proxies for climate reconstructions in northern Patagonia? J. Geophys. Res., Biogeosci. 121 (3), 767–776.

Liu, X., Xu, G., Grießinger, J., An, W., Wang, W., Zeng, X., Wu, G., Qin, D., 2014. A shift in cloud cover over the southeastern Tibetan Plateau since 1600: evidence from regional tree-ring $\delta^{18}O$ and its linkages to tropical oceans. Quat. Sci. Rev. 88, 55–68.

McCarroll, D., Loader, N.J., 2004. Stable isotopes in tree rings. Quat. Sci. Rev. 23 (7), 771–801.

Mölg, T., Maussion, F., Scherer, D., 2014. Mid-latitude westerlies as a driver of glacier variability in monsoonal High Asia. Nat. Clim. Change 4 (1), 68–73.

Miehe, G., Miehe, S., Will, M., Opgenoorth, L., Duo, L., Dorgeh, T., Liu, J., 2008. An inventory of forest relicts in the pastures of Southern Tibet (Xizang A.R. China). Plant Ecol. 194(2), 157–177.

Pang, H., Hou, S., Kaspari, S., et al., 2014. Influence of regional precipitation patterns on stable isotopes in ice cores from the central Himalayas. Cryosphere 8 (1), 289–301.

Risi, C., Bony, S., Vimeux, F., Jouzel, J., 2010. Water-stable isotopes in the LMDZ4 general circulation model: model evaluation for present-day and past climates and applications to climatic interpretations of tropical isotopic records. J. Geophys. Res., Atmos. 115 (D12). https://doi.org/10.1029/2009jd013255.

Risi, C., Ogée, J., Bony, S., Bariac, T., Raz-Yaseef, N., et al., 2016. The water isotopic version of the land-surface model ORCHIDEE: implementation, evaluation, sensitivity to hydrological parameters. Hydrol. Curr. Res. 7 (3), 258. https://doi.org/10.4172/2157-7587.1000258.

Sano, M., Ramesh, R., Sheshshayee, M.S., Sukumar, R., 2011. Increasing aridity over the past 223 years in the Nepal Himalaya inferred from a tree-ring $\delta^{18}O$ chronology. Holocene 22 (7), 809–817.

Sano, M., Tshering, P., Komori, J., Fujita, K., Xu, C., Nakatsuka, T., 2013. May–September precipitation in the Bhutan Himalaya since 1743 as reconstructed from tree ring cellulose $\delta^{18}O$. J. Geophys. Res., Atmos. 118 (15), 8399–8410.

Sano, M., Dimri, A.P., Ramesh, R., Xu, C., Li, Z., Nakatsuka, T., 2017. Moisture source signals preserved in a 242-year tree-ring $\delta^{18}O$ chronology in the western Himalaya. Glob. Planet. Change 157, 73–82.

Shi, C., Masson-Delmotte, V., Risi, C., Eglin, T., Stievenard, M., Pierre, M., Wang, X., Gao, J., Bréon, F., Zhang, Q., Daux, V., 2011. Sampling strategy and climatic implications of tree-ring stable isotopes on the southeast Tibetan Plateau. Earth Planet. Sci. Lett. 301 (1), 307–316.

Sodemann, H., Schwierz, C., Wernli, H., 2008. Interannual variability of Greenland winter precipitation sources: Lagrangian moisture diagnostic and North Atlantic Oscillation influence. J. Geophys. Res., Atmos. 113, D03107. https://doi.org/10.1029/2007JD008503.

Stohl, A., Forster, C., Frank, A., Seibert, P., Wotawa, G., 2005. Technical note: the Lagrangian particle dispersion model FLEXPART version 6.2. Atmos. Chem. Phys. 5, 2461–2474.

Su, Z., Wen, J., Dente, L., et al., 2011. The Tibetan Plateau observatory of plateau scale soil moisture and soil temperature (Tibet-Obs) for quantifying uncertainties in coarse resolution satellite and model products. Hydrol. Earth Syst. Sci. 15 (7), 2303–2316.

Szejner, P., Wright, W.E., Babst, F., Belmecheri, S., Trouet, V., Leavitt, S.W., Ehleringer, J.R., Monson, R.K., 2016. Latitudinal gradients in tree ring stable carbon and

oxygen isotopes reveal differential climate influences of the North American Monsoon System. J. Geophys. Res., Biogeosci. 121, 1978–1991.
Thompson, L.G., Yao, T., Davis, M.E., et al., 2018. Ice core records of climate variability on the Third Pole with emphasis on the Guliya ice cap, western Kunlun Mountains. Quat. Sci. Rev. 188, 1–14.
Thompson, L.G., Yao, T., Mosley-Thompson, E., Davis, M.E., Henderson, K.A., Lin, P.-N., 2000. A high-resolution millennial record of the South Asian monsoon from Himalayan ice cores. Science 289 (5486), 1916–1919.
Tang, K., Feng, X., 2001. The effect of soil hydrology on the oxygen and hydrogen isotopic compositions of plants' source water. Earth Planet. Sci. Lett. 185 (3), 355–367.
Tian, L., Yao, T., Schuster, P., White, J., Ichiyanagi, K., Pendall, E., Pu, J., Yu, W., 2003. Oxygen-18 concentrations in recent precipitation and ice cores on the Tibetan Plateau. J. Geophys. Res. 108 (D9). https://doi.org/10.1029/2002JD002173.
Tian, L., Yao, T., Wen, R., Weng, Y., Zhao, Z., Qu, D., 2012. A primary recognition on the climatic significance of the ice core isotope record in Naimon'Nyi of western Tibetan Plateau. Q. Sci. 32 (1), 46–52 (in Chinese with English abstract).
Uppala, S.M., Kållberg, P.W., Simmons, A.J., et al., 2005. The ERA-40 re-analysis. Q. J. R. Meteorol. Soc. 131 (612), 2961–3012.
van der Sleen, P., Groenendijk, P., Zuidema, P.A., 2015. Tree-ring δ^{18}O in African mahogany (*Entandrophragma utile*) records regional precipitation and can be used for climate reconstructions. Glob. Planet. Change 127, 58–66.
Volland, F., Pucha, D., Bräuning, A., 2016. Hydro-climatic variability in southern Ecuador reflected by tree-ring oxygen isotopes. Erdkunde, 69–82.
Wang, X., Wang, T., Guo, H., Liu, D., Zhao, Y., Zhang, T., Liu, Q., Piao, S., 2017. Disentangling the mechanisms behind winter snow impact on vegetation activity in northern ecosystems. Glob. Change Biol. 24, 1651–1662. https://doi.org/10.1111/gcb.13930.
Wernicke, J., Hochreuther, P., Grießinger, J., Zhu, H., Wang, L., Bräuning, A., 2017. Multi-century humidity reconstructions from the southeastern Tibetan Plateau inferred from tree-ring δ^{18}O. Glob. Planet. Change 149, 26–35.
West, A.G., Hultine, K.R., Burtch, K.G., Ehleringer, J.R., 2007. Seasonal variations in moisture use in a piñon–juniper woodland. Oecologia 153 (4), 787–798.
Xu, C., Sano, M., Dimri, A., Ramesh, R., Nakatsuka, T., Shi, F., Guo, Z., 2018. Decreasing Indian summer monsoon in northern Indian sub-continent during the last 180 years: evidence from five tree cellulose oxygen isotope chronologies. Clim. Past 14, 653–664.
Yang, W., Yao, T., Guo, X., Zhu, M., Li, S., Kattel, D.B., 2013. Mass balance of a maritime glacier on the southeast Tibetan Plateau and its climatic sensitivity. J. Geophys. Res., Atmos. 118 (17), 9579–9594.
Yao, T., Masson-Delmotte, V., Gao, J., Yu, W.S., Yang, X.X., Risi, C., Sturm, C., Werner, M., Zhao, H., He, Y., Ren, W., Tian, L., Shi, C., Hou, S., 2013. A review of climatic controls on δ^{18}O in precipitation over the Tibetan Plateau: observations and simulations. Rev. Geophys. 51 (4), 525–548.
Yoshimura, K., Kanamitsu, M., Noone, D., Oki, T., 2008. Historical isotope simulation using reanalysis atmospheric data. J. Geophys. Res., Atmos. 113, D19108. https://doi.org/10.1029/2008JD010074.
Yu, W., Yao, T., Tian, L., Ma, Y., Wen, R., Devkota, L., Wang, W., Qu, D., Chhetri, T.B., 2016a. Short-term variability in the dates of the Indian monsoon onset and retreat on the southern and northern slopes of the central Himalayas as determined by precipitation stable isotopes. Clim. Dyn. 47 (1–2), 159–172.
Yu, W., Tian, L., Risi, C., Yao, T., Ma, Y., Zhao, H., Zhu, H., He, Y., Xu, B., Zhang, H., Qu, D., 2016b. δ^{18}O records in water vapor and an ice core from the eastern Pamir Plateau: implications for paleoclimate reconstructions. Earth Planet. Sci. Lett. 456, 146–156.
Zeng, X., Liu, X., Evans, M.N., Wang, W., An, W., Xu, G., Wu, G., 2016. Seasonal incursion of Indian Monsoon humidity and precipitation into the southeastern Qinghai–Tibetan Plateau inferred from tree ring δ^{18}O values with intra-seasonal resolution. Earth Planet. Sci. Lett. 443, 9–19.
Zhang, Y.P., Jiang, Y., Wang, B., Jiao, L., Wang, M.C., 2018. Seasonal water use by *Larix principis-rupprechtii* in an alpine habitat. For. Ecol. Manag. 409, 47–55.
Zhao, H., Xu, B., Li, Z., Wang, M., Li, J., Zhang, X., 2017. Abundant climatic information in water stable isotope record from a maritime glacier on southeastern Tibetan Plateau. Clim. Dyn. 48 (3–4), 1161–1171.